magnetite within the pyroxene; however, these appear to have been formed on the fracture surfaces at the same time as the magnetite and Fe-sulfide phases associated with the carbonate globule.

22. J. L. Kirschvink, in *Biomagnetism: An Interdisciplinary Approach*, S. Williamson, Ed. (Plenum, New York, 1983), pp. 501-532.
23. The intact sample was mounted at one end of a quartz-glass fiber 15 cm long and 1 mm in diameter, which had been cleaned in concentrated HCl. It was attached to this fiber using cyanoacrylate cement that had been passed through a 0.2-μm syringe filter to remove ferromagnetic impurities (Fig. 1A). The opposite end of the fiber was attached to the vertex of a flat quartz-glass triangle, such that the open face of the carbonate layer on the fracture surface was aligned parallel to the triangle's surface. The edge of the triangle opposite from the fiber attachment was fused to an elongate hook, allowing the assembly to be suspended vertically on a thin (~200-g test) nylon fishing line U-loop. This loop was wound on a Teflon spool attached to a small computer-controlled stepping motor mounted on the ceiling of the clean-lab facility, and held directly above the room-temperature access port of the superconducting magnetometer. With this assembly, the sample could be raised and lowered smoothly from the sample loading position to a pair of computer-controlled solenoids for the demagnetization and rock magnetic experiments, and to the center of a three-axis superconducting moment magnetometer (a 2G Enterprises® model 570, with DC-biased SQuIDs). A horizontal arrow marked on the quartz triangle was aligned with the $+X$ direction of the superconducting moment magnetometer; vertical down was $+Z$, and the $+Y$ direction formed the third axis of a right-handed orthogonal coordinate system. We were able to obtain replicate measurements to better than 1% intensity, and 0.5° in direction, on magnetic moments as weak as 10^{-12} A m^{-2}, equivalent to the saturation remanence produced by ~20 picograms of single-domain (SD) magnetite.
24. This separation was done using a 150-μm-thick diamond-impregnated copper wafering saw. The flat surface of the carbonate-bearing grain was first glued to a thin Pyrex cover slip such that it was parallel to the surface of the quartz-glass triangle. The magnetic moment of this new assembly was indistinguishable from that measured prior to addition of the cover slip and the additional cement, confirming that they were both nonmagnetic. The other surface of the Pyrex cover slip was then bound to the surface of a cylindrical brass stub with a temperature-sensitive adhesive that had been filtered in acetone to remove ferromagnetic contaminants. The orientation of the quartz fiber was marked on the brass surface. Shortly after we began our first cut, the bond between the cyanoacrylic cement and the cover slip gave way. This left a small notch in the sample at the boundary between the pyroxene grains (Fig. 1A). By remeasuring the NRM of the sample after this step, we were able to calculate by difference the NRM vector that had been held by the material removed in the cut. Next, we fixed the flat surface of the carbonate-bearing layer directly to the brass stub with the adhesive, which held properly during the remainder of the wafering process. This last cut was adjusted slightly so that most material was removed from the larger grain, leaving a 2.2-mg fragment of the small pyroxene grain on the brass stub (Fig. 1D). While it was still bound to the stub, we then used the cyanoacrylate to cement a second quartz-glass triangle and fiber assembly to the this new fragment, with a relative orientation identical to that of the first sample. It was then freed from the brass stub by heating briefly to 110°C, and washed with filtered acetone to dissolve traces of the adhesive. The sawing procedure left a 1.6-mg fragment of the carbonate-bearing grain attached to the larger pyroxene grain. After measurement of the NRM, we were able to break this free with a nonmagnetic ceramic scalpel blade, and by remeasuring the NRM vector, were able to recover by difference the NRM vector of this small chip. The final weight of the pyroxene grain was 12.7 mg, implying that a total of 3.4 mg of the sample was lost in both sawing operations.
25. J. L. Gooding, *Icarus* **99**, 28 (1992).
26. R. F. Butler, *Paleomagnetism: Magnetic Domains to Geologic Terranes* (Blackwell, Boston, 1992).
27. AF demagnetization was not continued to higher levels for the small pyroxene grain because the intensity became weak and it had a linear decay toward the origin. Thermal demagnetization experiments were not done, because of the possibility of irreversible mineralogical changes on some of the Fe-S minerals, such as the iron monosulfides reported by McKay *et al.* (*1*).
28. J. L. Kirschvink, *Geophys. J. R. Astron. Soc.* **62**, 699 (1980).
29. P. L. Mcfadden and M. W. McElhinny, *Earth Planet. Sci. Lett.* **87**, 161 (1988).
30. C. K. Shearer *et al.*, *Geochim. Cosmochim. Acta* **60**, 2921 (1996).
31. M. J. Dekkers, *Phys. Earth Planet. Inter.* **52**, 376 (1988).
32. H. P. Johnson *et al.*, *Geophys. J. R. Astron. Soc.* **41**, 1 (1975).
33. S. Cisowski, *Phys. Earth Planet. Inter.* **26**, 56 (1981).
34. We thank D. McKay and E. K. Gibson for our sample of ALH84001, P. Carpenter for assistance with the SEM, and G. R. Rossman for help with the delicate sawing operation. H.V. acknowledges financial support from the U.S. National Research Council. We made extensive use of the software provided by C. Jones (cjones@mantle.colorado.edu) for the analysis and presentation of paleomagnetic data. B. C. Murray, J. Eiler, and D. A. Evans made helpful suggestions on the manuscript. This is contribution no. 5897 from the Division of Geological and Planetary Sciences of the California Institute of Technology.

31 January 1997; accepted 20 February 1997

Low-Temperature Carbonate Concretions in the Martian Meteorite ALH84001: Evidence from Stable Isotopes and Mineralogy

John W. Valley, John M. Eiler, Colin M. Graham,
Everett K. Gibson, Christopher S. Romanek, Edward M. Stolper

The martian meteorite ALH84001 contains small, disk-shaped concretions of carbonate with concentric chemical and mineralogical zonation. Oxygen isotope compositions of these concretions, measured by ion microprobe, range from $\delta^{18}O = +9.5$ to $+20.5$‰. Most of the core of one concretion is homogeneous (16.7 ± 1.2‰) and over 5‰ higher in $\delta^{18}O$ than a second concretion. Orthopyroxene that hosts the secondary carbonates is isotopically homogeneous ($\delta^{18}O = 4.6 \pm 1.2$‰). Secondary SiO_2 has $\delta^{18}O = 20.4$‰. Carbon isotope ratios measured from the core of one concretion average $\delta^{13}C = 46 \pm 8$‰, consistent with formation on Mars. The isotopic variations and mineral compositions offer no evidence for high temperature (>650°C) carbonate precipitation and suggest non-equilibrium processes at low temperatures (<~300°C).

Carbonate concretions in ALH84001 provide information on the nature of the ancient martian atmosphere and hydrosphere, and aspects of their composition and morphology have been proposed as evidence for primitive life on Mars (*1*). The temperatures of carbonate formation are uncertain, but central to these questions. Mineral equilibria and the morphology of magnetite inclusions in carbonate have been used to infer temperatures of over 650°C (*2*, *3*), in which case carbon-based life is unlikely. On the other hand, oxygen isotope compositions of carbonate and the magnetic properties of millimeter-scale subdomains in ALH84001 have been interpreted to indicate that the minerals formed at temperatures of 0° to 110°C (*4*, *5*); suggesting precipitation during weathering or alteration. Such conditions would be permissive of life as we know it.

The ALH84001 meteorite is composed dominantly of igneous orthopyroxene ($Mg_{0.70}Fe_{0.27}Ca_{0.03}SiO_3$) with minor clinopyroxene, olivine, chromite, pyrite, apatite or whitlockite, maskelynite (shock-produced feldspathic glass $An_{31}Ab_{63}Or_6$), and SiO_2 (*2*, *6*, *7*). The sample is highly fractured, probably from impacts while it was still on Mars (*6*, *7*). Secondary carbonates are precipitated in some of these fractures and as disseminated patches in brecciated orthopyroxene (*2*, *6*, *7*).

We analyzed two carbonate concretions for isotopic and chemical compositions from a group of 14 that are approximately co-planar within an area of 2 mm^2 (Fig. 1A). Concretion #1 appears to be two concretions grown together, each of which has concentric core-to-rim chemical variations from $Ca_{0.15}Mg_{0.45}Fe_{0.40}CO_3$ to nearly pure $MgCO_3$ [Figs. 1C, 1D, 2, and figure 1 of

---

J. W. Valley, Department of Geology and Geophysics, University of Wisconsin, Madison, WI 53706, USA.
J. M. Eiler and E. M. Stolper, Division of Geological and Planetary Sciences, California Institute of Technology, Pasadena, CA 91125, USA.
C. M. Graham, Department of Geology and Geophysics, Edinburgh, EH9 3JW, Scotland, UK.
E. K. Gibson, NASA–Johnson Space Center, Houston, TX 77058, USA.
C. S. Romanek, Savannah River Ecology Laboratory, University of Georgia, Drawer E, Aiken, SC 29802, USA.

(*2*)]. This variation is not continuous; there is an abrupt compositional break between the orange, continuously zoned, Fe-rich core ($X_{Mg} \leq 0.7$ in Fig. 2) and the ~10-μm-wide mantle of nearly pure magnesite ($MgCO_3$, Mg-rich in Fig. 1D). Thin, black, Fe-rich rims separate the core from the mantle and the mantle from orthopyroxene. The Fe-rich character of the rims derives, at least in part, from submicroscopic grains of Fe oxide (magnetite) and sulfide that may also be trace constituents within the orange carbonate (*1*). The concretions are thin disks and the concentric zonation is seen optically only at the outer perimeter of the disk. These observations suggest that the concretions grew radially outward from the center along preexisting cracks. Some of the compositional zones are offset or truncated by microfractures, demonstrating that a second fracturing event postdated the precipitation of carbonates (*6, 7*). A thin (1 to 10 μm) vein of SiO_2 cuts across concretion #1 (orange in Fig. 1E). SiO_2 is also found as irregularly shaped grains within orthopyroxene.

Previous oxygen and carbon isotope analyses of carbonate in martian meteorites have been made by chemical dissolution or thermal decomposition of whole-rock powders or mineral separates. For ALH84001, values varied from $\delta^{18}O = -9$ to $+26‰_{VSMOW}$ and $\delta^{13}C = -21$ to $+53‰_{PDB}$ [Fig. 3 (*4, 8, 9*)], but most values were $\delta^{18}O = 17.5 \pm 2.7‰$ (1 SD, $n = 7$) and $\delta^{13}C = 36 \pm 10‰$ (1 SD, $n = 9$). Both low $\delta^{18}O$ and low $\delta^{13}C$ (<0‰) values have been reported (Fig. 3), although it is unclear which components of the meteorite (or minor terrestrial contaminants) these low values reflect, whether they accurately measure a single component of the meteorite, and to what degree the meteorite is isotopically heterogeneous on a microscale. The question of homogeneity is important vis-à-vis the thermal history of the meteorite. Chemical and isotopic gradients diffuse away more quickly at higher temperatures and, given knowledge of appropriate diffusivities, the presence or absence of such gradients can be used as quantitative constraints on thermal history.

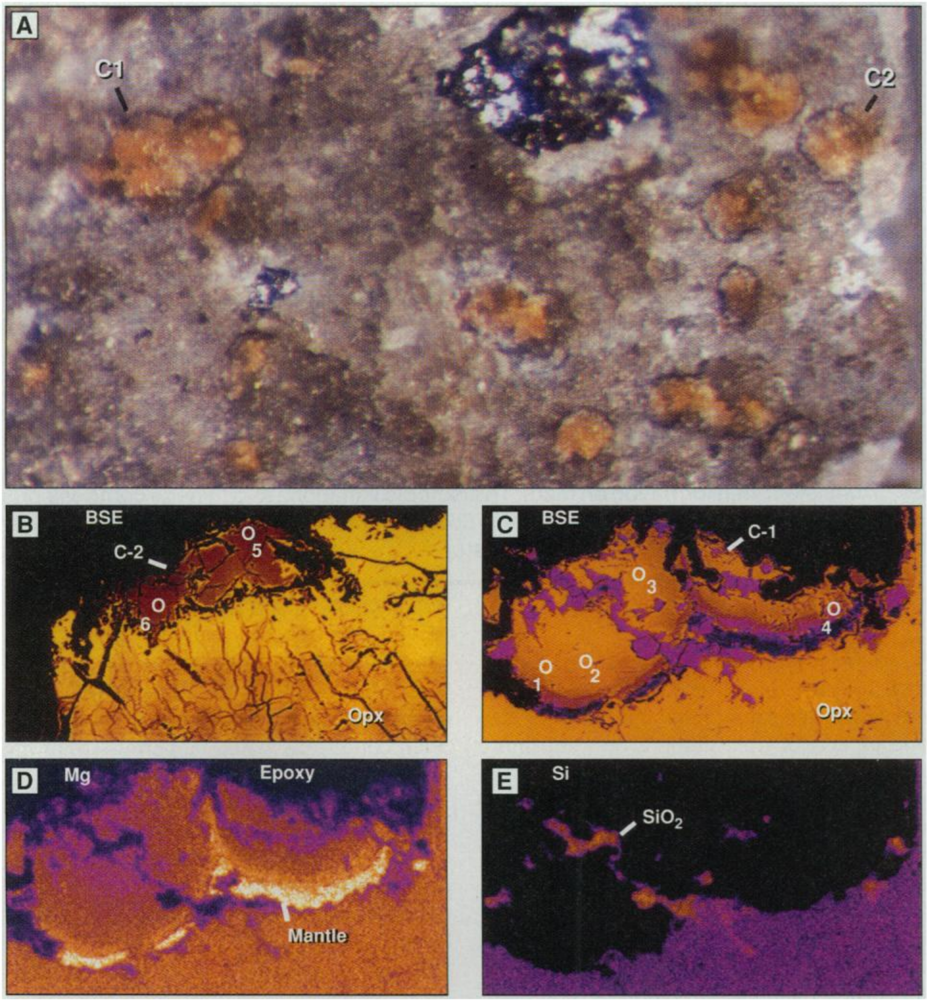

Fig. 1. (**A**) Photograph of freshly broken surface of ALH84001 showing orange carbonate concretions and host orthopyroxene. The dark crystals are chromite. Each concretion has thin black rims, rich in magnetite and sulfides, on either side of a white magnesite mantle (*1, 6, 7*). Concretions #1 and #2 were analyzed in situ for stable isotope ratio and chemical composition. FOV = 1.5 mm. (**B** and **C**) Backscattered electron (BSE) images of concretion #1 (C) and #2 (B). The locations of ion probe spots #1 to 6 are shown (other analyses were made deeper in the sample after repolishing). (**D** and **E**) Images of chemical composition of the polished surface of carbonate concretion #1 and host orthopyroxene (Opx) before ion probe analysis. Part of the concretion is covered by epoxy (toward top of picture). (D) shows Mg and (E) shows Si. The rounded, composite shape of this concretion is best seen in the image of Mg (D), the white band is the magnesite mantle that rims the concretion boundary with orthopyroxene and divides this concretion into two nearly round subconcretions that have apparently grown together. The left side of the concretion is nearly round and fully exposed, but only the lower half of the right side is exposed. In (B) to (E) hot colors (white or yellow) indicate the highest concentrations or average atomic numbers (BSE), and blue or black indicates the lowest concentrations. Field of view is = 256 μm.

Ion microprobe–secondary ion mass-spectrometry (SIMS) permits in situ analysis of oxygen and carbon isotope ratios in small samples (5 ng, 20- to 30-μm-diameter pits, 6 to 8 μm deep) of carbonate and silicate minerals (*10–14*). Sample sizes are 10^3 to 10^6 times smaller than previous bulk analyses, allowing us to analyze several spots in a single concretion, the largest of which measures 250 μm in its greatest dimension and is estimated to weigh less than 2 μg. These in situ measurements can be correlated with chemical, spatial, and textural information.

We made 20 analyses of $\delta^{18}O$ and 4 of $\delta^{13}C$ in the meteorite. We also made over 500 analyses of 12 carbonate standards to assess analytical precision, stability, and standardization (*12–14*). We analyzed seven spots for $\delta^{18}O$ in concretion #1 and two in #2, and four spots for $\delta^{13}C$ in concretion #1 (Table 1). All analyses are of orange, Fe-rich magnesites in the concretion cores, except analysis #4, which overlaps the white magnesite mantle. The average chemical compositions of analyzed spots were determined using a focused electron microprobe beam on the rims of ion probe pits after analysis and are in good agreement with defocused beam analyses from before ion probe analysis (Table 1 and Fig. 2).

The average $\delta^{13}C$ value was $+46 \pm 8‰$. This composition is based on data only from the beginning of the four analyses because heterogeneities present at depths of 1 to 4 μm were attributed to contamination or reduced carbon in the sample (*13, 14*). The resultant total counts for these analyses are low and less precise than would otherwise be possible. All four analyses agree within 1 SD of each analysis. The average value is at the upper end of the range of previously measured values (Fig. 3). On Earth, values of $\delta^{13}C$ in carbonates are typically near 0‰, values above +20‰ are rare for any mineral [in some cases forming in carbonates as a result of bacterial methanogenesis (*15*)], and we know of no values above +35‰ (*15, 16*). Thus, the carbon isotope ratios of carbonate in ALH84001 are not consistent with any known terrestrial materials and indicate that they are extraterrestrial, as concluded previously based on dissolution measurements (*4*) and the presence of fractures that are presumably of impact origin that cross-cut the carbonates displacing chemical zonation (*1, 6, 7*). These $\delta^{13}C$ values, which are 40 to 50‰ higher than average values on Earth, are consistent with precipitation from or equilibration with a reservoir having a $\delta^{13}C$ value similar to that estimated for the atmosphere of Mars (Fig. 3), which is thought to be 30 to 50‰ higher than on Earth (*17, 18*).

In concretion #1, five of the six $\delta^{18}O$ values of orange Fe-rich magnesite are indistinguishable within analytical precision at 16.7 ± 1.2‰ (Fig. 3). The sixth spot yielded a $\delta^{18}O$ value of 12.2 ± 1.1‰. A seventh spot (pit #4) overlapped onto the white magnesite mantle and yielded the highest $\delta^{18}O$ value of 20.6 ± 1.3‰. The two analyses of concretion #2 (9.5, 13.5‰) are within analytical precision of the one low $\delta^{18}O$ spot in concretion #1 (Fig. 3). The ion probe results compare favorably with most of the previous bulk analyses, but the spatial resolution of the ion probe documents heterogeneity that could only previously be inferred. No attempt was made to analyze the magnesite mantles because those in our specimen are smaller than the size of the ion beam. However, the relatively high $\delta^{18}O$ value of the spot that overlaps the magnesite mantle (#4, Table 1) suggests that the mantle has an even higher $\delta^{18}O$ value, consistent with the results of Romanek *et al.* (*4*), who suggested that the $\delta^{18}O$ of the magnesite is 9‰ higher than that of the core of the concretions on the basis of stepwise acid dissolution experiments. There is no correlation of $\delta^{18}O$ value with chemical composition for the eight analyses of orange carbonate. Although the number of analyses is limited, our eight $\delta^{18}O$ values have a bimodal distribution (9.5 to 13.5‰ and 15.5 to 18.7‰).

On Earth, $\delta^{18}O$ values as high (≥16‰) as those that we have measured in ALH84001 carbonates are only found in rocks that have interacted with isotope reservoirs formed at low temperatures [<100°C (*16*)]. A simple interpretation (*4, 19, 20*) would be that the $\delta^{18}O$ values of aqueous fluids on Mars are related by processes of exchange to those of martian igneous rocks, in which case the elevated $\delta^{18}O$ values in carbonate concretions reflect low temperatures (<∼100°C) of precipitation. However, this reasoning cannot firmly constrain the temperature of carbonate formation until the $\delta^{18}O$ of the martian atmosphere or hydrosphere is known (*21*), and we thus sought other evidence to determine the formation temperatures of carbonates in ALH84001.

Ten analyses of $\delta^{18}O$ in orthopyroxene demonstrate that it is homogeneous (4.6 ± 1.2‰). One analysis of SiO_2 from an irregular 40- by 50-μm grain enclosed by pyroxene yielded a $\delta^{18}O$ value of 20.4 ± 0.9‰ (*13*). It is not certain if this SiO_2 grain is related to maskelynite (or its precursor plagioclase) or to other glasses predating carbonate (*6, 7*), or is related to the post-concretion SiO_2 precipitating event that formed the vein in Fig. 1E.

There is no textural evidence to indicate equilibration of SiO_2 and other minerals, but if SiO_2 is assumed to be in isotopic equilibrium with orthopyroxene, then the measured $\delta^{18}O$ values indicate that the temperature of SiO_2 precipitation was 144° ± 14°C (*22, 23*). Equilibration of SiO_2 and the relatively homogeneous core of concretion #1 would indicate a temperature of 125° to 205°C (*24–27*). Equilibration temperatures implied by coexisting carbonate and orthopyroxene are similarly low, but variable: ∼170°C for the dominant carbonate in concretion #1 and ∼310°C for the average carbonate in concretion #2. These temperatures only have meaning if the various phases are in isotopic equilibrium, yet the heterogeneity among carbonates demonstrates a lack of isotopic equilibration at the scale of less than 1 mm and the contact between the magne-

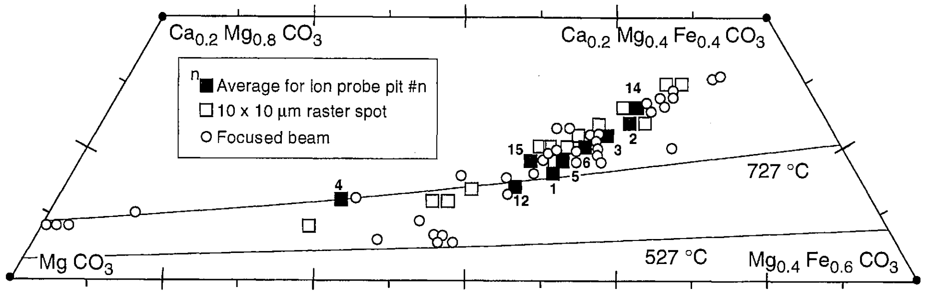

Fig. 2. Compositions of carbonates in concretions #1 and #2 in the Ca-Mg-Fe system measured by electron microprobe. Circles are analyses of 5-μm spots (beam focused to 1 μm), open squares are analyses of 10 by 10 μm areas, and solid squares are average compositions of 20-μm-diameter spots analyzed for oxygen isotope ratio by ion microprobe. Carbonates are not stable above the lines shown for 527° and 727°C (*29*).

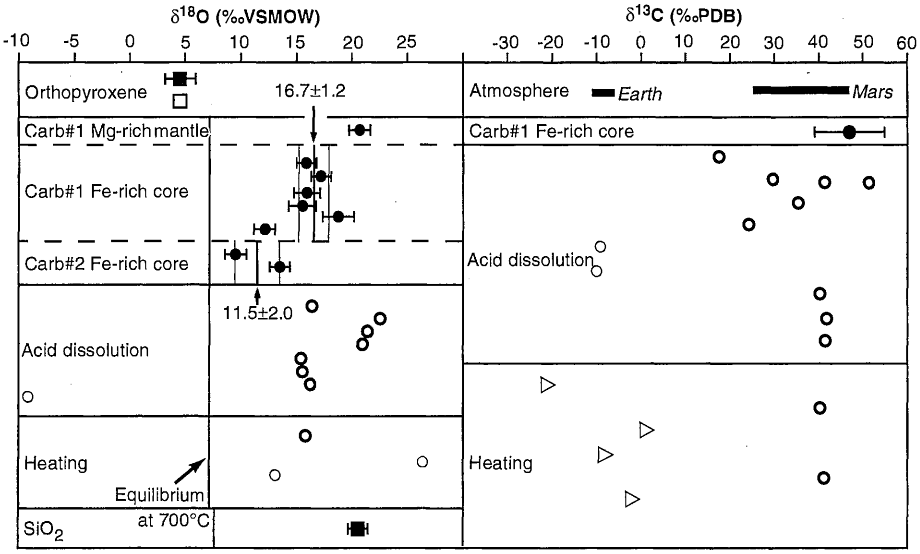

Fig. 3. Values of $\delta^{18}O$ and $\delta^{13}C$ measured in the martian meteorite ALH84001 in situ by ion microprobe (solid symbols, this study), and in powders by acid dissolution, step-heating, or fluorination [open symbols (*4, 9, 44*)]. Values shown in light type are suspected of contamination or fractionation. Samples are: carbonate (circles), silicates (squares), and suspected organic matter (triangles). The vertical lines at $\delta^{18}O \sim 7‰$ represent the value for carbonate or quartz in equilibrium with orthopyroxene at high temperature (>600°C). The $\delta^{13}C$ estimated for the atmosphere on Mars and Earth are also shown (*16–18*).

site mantle and orange carbonate may contain a disequilibrium isotopic gradient over distances of <10 μm [and possibly <1 μm (*4*, *7*)]. In any case, the intermineral oxygen isotope fractionations are not consistent with equilibration at the high temperatures previously inferred from the major element chemistry of the carbonates (>650°C).

Two opposed hypotheses can be examined to determine if they explain the geochemical and mineralogical features associated with carbonate concretions in ALH84001: (i) Precipitation of carbonate at high temperatures possibly over a short time period. This might occur during a meteorite impact and subsequent hydrothermal activity in which case a range of equilibration temperatures could be represented by different carbonates (*2*). (ii) Low-temperature nonequilibrium precipitation, such that isotopic and chemical disequilibrium during crystallization will be maintained because rates of reactions and solid-state diffusion are low.

The evidence favoring a high temperature origin of the carbonate concretions comes from major element analysis of mineral composition and mineral equilibria (*2*, *6*), and from textures in nanometer-scale magnetite grains within the carbonate (*3*). Harvey and McSween (*2*) estimated that the carbonates precipitated at temperatures of over 650°C on the basis of their analyses of carbonates in the calcite-magnesite- siderite system. This estimate assumes that: (i) the minerals were in chemical equilibrium at the time of formation, (ii) equilibrium compositions have been preserved, and (iii) that the analyses represent homogeneous phases. These assumptions can be applied to other minerals in ALH84001 as a test of the hypothesized high-temperature origin for carbonate.

Most of our analyses of carbonate in ALH84001 fall within the two phase region (solvus) of ankerite-magnesite immiscibility at 700°C (Fig. 2). Our analyses and previous studies (*2*, *6*, *7*) show that these more Ca-rich compositions are common in the cores of carbonate concretions. If the previously reported compositions in the range of X_{Ca} = 0.2 to 0.3 (*2*) represent homogeneous phases, equilibrium is only possible if carbonates precipitated at temperatures of $>\sim$1000°C (*28*, *29*). These very high temperatures are inconsistent with several other features of the concretions: First, pyrite is a primary mineral in the meteorite (*6*). The equilibria, pyrite = pyrrhotite + S, sets an upper temperature limit for pyrite of 750°C (*30*). Second, magnesite, forsterite-rich olivine, and enstatite-rich orthopyroxene occur as touching phases in ALH84001 [see figure 2 of (*2*)]. The equilibria enstatite + magnesite = forsterite + CO_2 would be at 550°C (*31*) in the presence of nearly pure CO_2 at P = 0.2 GPa (equivalent to a depth of over 50 km on Mars). This temperature is an upper limit. Shallower depths or aqueous fluids could reduce the stability of magnesite + SiO_2 to a maximum of 300°C or less (*31*). Finally, several other metamorphic reactions would occur under conditions of high temperature equilibration and a number of metamorphic minerals that have not been reported in ALH84001 would be expected along grain boundaries (for example, wollastonite, zoisite, scapolite, grossular, diopside, tremolite, anthophyllite, and talc). Thus, if equilibrium is assumed, there is no self-consistent interpretation, and this suggests either that the carbonates are metastable or the analyses represent mixtures of fine-grained phases.

The rates of fluid-hosted metamorphic reactions are known to be rapid at high temperatures, such that if carbonate compositions represent super-solvus temperatures, the above-discussed reactions could be expected to occur at grain boundaries over the time scales of minutes to hours (*32*). Studies of high-temperature carbonate precipitated during terrestrial impact events confirm this expectation, showing them to be intimately associated with shock-produced glass and, where carbonate touches silicate in host lithologies, the expected high-temperature metamorphic minerals occur [for example, clinopyroxene and larnite (*33*)]. The carbonates in ALH84001 show no similar reaction relations with adjacent host phases.

Table 1. Chemical composition measured by electron microprobe and stable isotope ratio measured by ion microprobe of 20-μm-diameter spots in carbonate concretions #1 and #2 and silicate minerals from ALH84001.

Analysis spot	X_{Mg}*	X_{Ca}	X_{Fe}	X_{Mn}	$\delta^{18}O$ (‰)	±1 SD (‰)†
1 concretion 1	0.598	0.084	0.312	0.006	15.9	1.3
2 concretion 1	0.522	0.121	0.343	0.014	17.2	1.0
3 concretion 1	0.546	0.110	0.335	0.009	12.2	1.1
4 concretion 1	0.747	0.062	0.188	0.003	20.6	1.3
12 concretion 1	0.627	0.071	0.299	0.003	15.9	1.2
14 concretion 1	0.507	0.127	0.350	0.015	15.5	1.2
15 concretion 1	0.586	0.085	0.295	0.034	18.7	1.3
5 concretion 2	0.578	0.094	0.317	0.011	9.5	1.1
6 concretion 2	0.566	0.104	0.323	0.008	13.5	1.2
SiO_2					20.4	0.9

$\delta^{18}O$ of orthopyroxene: 2.6, 3.1, 5.6, 4.9, 3.2, 6.4, 5.6, 4.7, 5.6, 4.0‰; average = 4.6 ± 1.2‰

$\delta^{13}C$ of carbonate: 49, 36, 45, 55‰; average = 46 ± 8‰

*X = molar fraction of cations in carbonate. †Values of 1 standard deviation (SD) dictated by counting statistics for carbonate analyses #1 to 15. For multiple analyses ($N > 1$), external precision about the mean is reported.

If temperatures were high, then exchange by diffusion would cause homogenization of isotopic and chemical gradients (*34*). The sharpest gradients documented in ALH84001 are in Mg/Fe ratios between the nearly pure magnesite of the white concretion mantles and the orange Fe-rich magnesite of the cores [occurring over a length scale of $\sim$1 μm (*7*)]. The $\delta^{18}O$ value of pit #4 (20.6‰, Table 1) suggests that there may also be large gradients in $\delta^{18}O$ across magnesite mantles (Table 1). A gradient of 9‰ was inferred by dissolution experiments (*4*). At 1000°C, experimental data suggest that gradients in cation composition would homogenize in 1 to 100 days (*35*) and the inferred differences in $\delta^{18}O$ would homogenize in 10 to 2500 min (*36*). However, at low temperatures ($\sim$100°C), compositional contrasts will be preserved in the absence of recrystallization. On Earth, gradients of 5 to 13‰ over 10 to 400 μm have only been documented from diagenetic and low-temperature (from <80° to 400°C) alteration environments (*10*, *37*, *38*). For >650°C igneous or metamorphic processes, measurable diffusion gradients are typically less than 2‰ (*10*, *39*). In addition, if temperatures were high, then fluids forming high $\delta^{18}O$ carbonates must also have had elevated $\delta^{18}O$ values and would be expected to have exchanged with the orthopyroxene along the boundary of cracks causing heterogeneity that is not observed. It is evident from these considerations that the mineralogy and isotopic values of the carbonate concretions and their relations to the host orthopyroxene cannot be reconciled with high-temperature equilibration.

The alternative hypothesis is that carbonates precipitated from a fluid at low temperatures. Such conditions are common on Earth, frequently forming minerals that are not equilibrated, either isotopically or chemically (*37*, *38*). Fine-scale oxygen isotope heterogeneity is readily formed and easily preserved at low temperatures where diffusion is slow, but requires a complex process of precipitation and rapid cooling if formed at high temperatures. Delicate mineral overgrowths and reaction textures such as observed in ALH84001 carbonates (*6*, *7*) are common in low temperature ($\leq$300°C) environments on Earth, and in many cases, sharp contrasts in chemical and isotopic composition (*37, 38*) are preserved at the same scale as that seen in the carbonate concretions.

There are well-documented situations where low-temperature (from <100° to 500°C) carbonate veins cut minerals without visible reaction, including orthopyroxene-bearing lithologies (*40*) and samples shattered by meteorite impact (*41*). It has been suggested that nearly pure CO_2 and high temperatures are necessary in order to prevent hydration reactions involving pyroxene at the time that carbonates were precipitated (*2*). However, carbonates can precipitate over a wide range of temperatures and from water-rich fluids without producing hydrated minerals (*40*).

Low-temperature carbonate minerals commonly form in apparent violation of equilibrium thermodynamics, including aragonite, and high-magnesium calcites and calcian dolomites (which are inside the solvus). If these minerals were assumed to form in stable equilibrium, one would erroneously conclude that the Earth's oceans exist at temperatures over 500°C and surface pressures of at least several thousand atmospheres. The kinetic processes that cause apparent disequilibrium are not well understood and can be either biogenic or abiogenic (*42*). The scale of observation is another factor; some carbonates are actually complex submicroscopic mixtures that require high-resolution transmission electron microscopy for proper characterization (*43*). It is not known if all of the carbonates reported from ALH84001 are truly homogeneous single phases at the submicrometer-scale, and textures characteristic of low-temperature growth may yet be found (*43*).

Thus, there are many well-studied and common terrestrial analogs for low-temperature processes that could form carbonate concretions, such as described in ALH84001. All of the chemical, mineralogical and isotopic evidence that we have presented are consistent with such a model. In contrast: (i) the isotopic data that we present are not consistent with high-temperature equilibration in ALH84001; (ii) there is no mineral, chemical, or phase equilibria evidence that indicates a self-consistent high-temperature (>650°C) genesis for the carbonate concretions in ALH84001; (iii) and well-studied high-temperature terrestrial analogs have features clearly inconsistent with those observed in ALH84001.

REFERENCES AND NOTES

---

1. D. S. McKay *et al.*, *Science* **273**, 924 (1996).
2. R. P. Harvey and H. Y. McSween Jr., *Nature* **382**, 49 (1996).
3. J. P. Bradley, R. P. Harvey, H. Y. McSween Jr., *Geochim. Cosmochim. Acta* **60**, 5149 (1996).
4. C. S. Romanek *et al.*, *Nature* **372**, 655 (1994).
5. J. L. Kirchvink, A. T. Maine, H. Vali, *Science* **275**, 1629 (1997).
6. D. W. Mittlefehldt, *Meteoritics* **29**, 214 (1994).
7. A. H. Treiman, *ibid.* **30**, 294 (1995).
8. $\delta^{18}O$ = 1000 [($^{18}O/^{16}O$-sample)/($^{18}O/^{16}O$-VSMOW) −1], where VSMOW is the international standard ocean water. $\delta^{13}C$ = 1000 [($^{13}C/^{12}C$-sample)/($^{13}C/^{12}C$-PDB) − 1] where PDB is the Pee Dee belemnite standard.
9. M. M. Grady, I. P. Wright, C. Douglas, C. T. Pillinger, *Meteoritics* **29**, 469 (1994); A. J. Jull, C. J. Eastoe, S. Xue, G. F. Herzog, *ibid.* **30**, 311 (1995); L. A. Leshin, S. Epstein, E. M. Stolper, *Geochim. Cosmochim. Acta* **60**, 2635 (1996).
10. J. W. Valley, C. M. Graham, B. Harte, J. M. Eiler, P. D. Kinny, *Rev. Econ. Geol.* **7**, in press.
11. J. M. Eiler, C. Graham, J. W. Valley, *Chem. Geol.* in press.
12. J. M. Eiler, J. W. Valley, C. M. Graham, *Lunar Planet. Sci.*, in press.
13. The sample, ALH84001,200, was cast in epoxy and polished. The sample was repolished twice during the analysis of carbonates (after analysis #6 and before #12) to remove 5 to 10 μm from its surface and reveal fresh material for analysis. Stable isotope analysis was made with a Cameca ims 4f ion micro probe at the University of Edinburgh using a high-energy offset (350 ± 25 eV for O, 250 ± 25 eV for C). The spot size was 20 μm for O and 30 to 40 μm for C by 6 to 8 μm deep (volume = $\sim 2000\ \mu m^3$, mass ≈ 5 ng of mineral for O). Analyses of standards had precisions (based on counting statistics) of ±1‰ (1 SD) for $^{18}O/^{16}O$ and ±1.5‰ for $^{13}C/^{12}C$. Sample analyses were comparable in precision for O, but C analyses of sample were truncated because of heterogeneities at depths of 1 to 4 μm (*14*). At the beginning of each sample $\delta^{13}C$ measurement, count rates, and isotope ratios were steady, but after 17 to 56 cycles (at depths of 1 to 4 μm), count rates increased and then decreased, and measured isotope ratios decreased by 48 ± 2‰. Since these sample analyses were bracketed by good analyses of carbonate standards, these changes must result from real differences in the sample at depth. Possible explanations include: contamination by epoxy or polishing materials, differences in chemical composition which affect count rate and α_{SIMS} ($\alpha_{sims} = R_{sims}/R_{true}$, where R = $^{18}O/^{16}O$ or $^{13}C/^{12}C$), or the presence of reduced carbon phases inherent to the sample with drastically lower $\delta^{13}C$. Only data from the initial, steady part of each depth profile were used to calculate $\delta^{13}C$ of the sample. Other analytical details are reviewed by (*10*). The 24 analyses were preceded by over 500 analyses of 12 homogeneous carbonate standards, nine of which are in the Ca-Mg-Fe system including: two calcites, two aragonites, Fe-dolomite, three Mg-bearing siderites (X_{Fe} = 0.96, 0.86, 0.71), magnesite, rhodochrosite, strontianite, and witherite (*12*). The matrix correction (α_{SIMS}) was found to vary nonlinearly across the Ca-Mg join, in the Ca-Mg-Fe system but to correlate well with X_{Fe} (for O, $\alpha = 0.968$ at $X_{Fe} = 1$ and 0.927 at $X_{Fe} = 0$; for C, $\alpha = 0.956$ at $X_{Fe} = 1$ and 0.932 at $X_{Fe} = 0$). The carbonate analyses in Table 1 are standardized against a Mg-rich siderite ($X_{Fe} = 0.71$) and the effect of solid solution is calibrated by the other eight Ca-Mg-Fe standards. Within the limited composition range of the orange carbonates we analyzed in ALH84001, differences in chemistry correspond to calibration differences of ±1‰. Small amounts of submicroscopic Fe oxides and sulfides may be present in the analyzed pits, especially in pit #4, but this is unlikely to have a significant effect on these data. The $\delta^{18}O$ analyses of orthopyroxene are calibrated against conventional analyses of this meteorite (*44*) as well as against ion probe analyses of a standard enstatite yielding the same value within uncertainty. The analysis of SiO_2 is standardized by ion probe data for Amelia albite (*11*). Chemical compositions were measured by electron microprobe in Edinburgh and in Madison using wavelength-dispersive spectrometers (WDS). Normal standardization and correction procedures were employed. The depth of x-ray excitation for quantitative chemical analysis is 5 μm such that the electron probe data represent nearly the same volume of sample as the 6 to 8 μm deep ion probe pits. Images of chemical composition (Fig. 1) were made in Madison with stage scans and WDS.
14. J. W. Valley, J. M. Eiler, C. M. Graham, E. K. Gibson, Jr., C. S. Romanek, *Lunar Planet. Sci.*, in press.
15. J. Veizer, W. T. Holser, C. K. Wilgus, *Geochim. Cosmochim. Acta* **44**, 579 (1980); T. F. Anderson and M. A. Aruthur, in *Stable Isotopes*, in *Sedimentary Geology*, SEPM Short Course **10**, 1 (1983); M. A. Aruthur *et al.*, *Annu. Rev. Earth Planet. Sci.* **15**, 47 (1987); E. M. Galimov, *Geochim. Cosmochim. Acta* **55**, 1697 (1991).
16. J. Hoefs, *Stable Isotope Geochemistry* (Springer, Berlin, ed. 4, 1997), p. 201.
17. R. H. Carr, M. M. Grady, I. P. Wright, C. T. Pillinger, *Nature* **314**, 248 (1985).
18. C. P. Harzmetz, I. P. Wright, C. T. Pillinger, in *Workshop on the Mars Surface and Atmosphere Through Time*, R. M. Haberle *et al.*, Eds. (*Tech. Rep. 92-02*, Lunar and Planetary Institute, Houston, TX, 1992), p. 67.
19. R. N. Clayton and T. K. Mayeda, *Geochim. Cosmochim. Acta* **52**, 925 (1988).
20. I. P. Wright, M. M. Grady, C. T. Pillinger, *ibid.* **56**, 817 (1992).
21. ______, *J. Geophy. Res.* **95**, 14,789 (1990); B. M. Jakosky, *Icarus* **94**, 14 (1991); *Geophy. Res. Lett.* **20**, 1591 (1993); S. M. Clifford, *J. Geophys. Res.* **98**, 10,973 (1993).
22. H. Chiba, T. Chacko, R. N. Clayton, J. R. Goldsmith, *Geochim. Cosmochim. Acta* **53**, 1985 (1989).
23. J. M. Rosenbaum, T. K. Kyser, D. Walker, *ibid.* **58**, 2653 (1994).
24. J. R. O'Neil, R. N. Clayton, T. K. Mayeda, *J. Chem. Phys.* **51**, 5547 (1969).
25. R. N. Clayton, J. R. O'Neil, T. K. Mayeda, *J. Geophys. Res.* **77**, 3057 (1972).
26. Z. D. Sharp and D. L. Kirschner, *Geochim. Cosmochim. Acta* **58**, 4491 (1994).
27. Isotope fractionations are calculated for calcite which approximates the value for intermediate magnesite-siderite solid solutions, and for quartz which approximates silica.
28. L. M. Anovitz and E. J. Essene, *J. Petrol.* **28**, 389 (1987); P. L. McSwiggen, *Phys. Chem. Miner.* **20**, 42 (1993).
29. P. M. Davidson, *Am. Miner.* **79**, 332 (1994).
30. J. R. Craig and S. D. Scott, in *Sulfide Phase Equilibria*, P. R. Ribbe, Ed. (vol. 1, *Reviews in Mineralogy Mineralogical Society of America*, Washington, DC 1974).
31. W. Johannes, *Am. J. Sci.* **267**, 1083 (1969); R. G. Berman, *J. Petrol.* **29**, 445 (1988).
32. B. J. Wood and J. V. Walther, *Science* **222**, 413 (1983).
33. I. Martinez, P. Agrinier, U. Schärer, M. Javoy, *Earth Planet. Sci. Lett.* **121**, 559 (1994).
34. J. Crank, *The Mathematics of Diffusion* (Clarendon Press, Oxford, 1975).
35. J. R. Farver and R. A. Yund, *Contr. Min. Petrol.* **123**, 77 (1996); D. J. Cherniak, *Eos* **76**, F683 (1995); W. G. Minarik and E. B. Watson, *Earth Planet. Sci. Lett.* **133**, 423 (1995).
36. T. F. Anderson, *J. Geophys. Res.* **76**, 3918 (1969); A. K. Kronenberg, R. A. Yund, B. J. Giletti, *Phys. Chem. Miner.* **11**, 101 (1984); J. R. Farver, *Earth Planet. Sci. Lett.* **121**, 575 (1994).
37. J. W. Valley and C. M. Graham, *Contrib. Miner. Petrol.* **109**, 38 (1991); J. W. Valley and C. M. Graham, *Science* **259**, 1729 (1993); J. W. Valley and C. M. Graham, *Contrib. Miner. Petrol.* **124**, 225 (1996); C. M. Graham, J. W. Valley, B. L. Winter, *Geochim. Cosmochim. Acta* **60**, 5101 (1996).
38. R. L. Hervig, L. B. Williams, I. K. Kirkland, F. J. Longstaffe, *Geochim. Cosmochim. Acta* **59**, 2537 (1995).
39. J. M. Eiler, J. W. Valley, L. P. Baumgartner, *ibid.* **57**, 2571 (1993); J. M. Eiler, J. W. Valley, C. M. Graham, L. P. Baumgartner, *Am. Miner.* **80**, 757 (1995).
40. J. Morrison and J. W. Valley, *Geology* **16**, 513 (1988); *J. Geol.* **99**, 559 (1991).
41. J. W. Valley, S. C. Komor, K. Baker, A. W. A. Jeffrey, I. R. Kaplan, A. Råheim, in *Crystalline Bedrock*, A. Boden and K. G. Eriksson, Eds. (Springer-Verlag,

New York, 1988), p. 156.

42. R. J. Reeder, Ed., *Carbonates: Mineralogy and Chemistry*, vol. 11, *Reviews in Mineralogy* (Mineralogical Society of America, Washington, DC, 1983); J. W. Morse, in *ibid.*, p. 227; I. Barnes and J. R. O'Neil, *Geochim. Cosmochim. Acta* **35**, 699 (1971); T. F. Anderson and M. A. Arthur, in *Stable Isotopes in Sedimentary Geology* (*Short Course 10*, Society of Economic Petrologists and Mineralogists, Dallas, TX, 1983), p. 1-1; J. M. Hayes, *Marine Geol.* **113**, 111 (1993); I. D. Clark and B. Lauriol, *Chem. Geol.* **102**, 217 (1992); T. McConnaughey, *Geochim. Cosmochim. Acta* **53**, 163 (1988).
43. R. J. Reeder, in *Minerals and Reactions at the Atomic Scale*, P. R. Buseck, Ed., *Rev. Miner.* **27**, 381 (1992).
44. R. N. Clayton and T. K. Mayeda, *Geochim. Cosmochim. Acta* **60**, 1999 (1996).
45. J. Craven aided in all aspects of the ion microprobe analysis in Edinburgh and M. Spicuzza analyzed carbonate standards in Madison. J. Muhl measured ion probe pit depth and volume by optical interferometer. B. Hess mounted and carefully polished the sample. J. Fournelle, T. Patterson, S. Burgess, and P. Hill assisted in electron microprobe analysis. M. Diman drafted the figures and B. Barker aided in photography. G. Rossman and R. Reeder donated carbonates as potential standards. We thank three anonymous reviewers for prompt, helpful comments. This research was supported by NSF, NASA, DOE and NERC.

10 February 1997; accepted 21 February 1997

Vacuum Squeezing of Solids: Macroscopic Quantum States Driven by Light Pulses

G. A. Garrett, A. G. Rojo, A. K. Sood,* J. F. Whitaker, R. Merlin†

Femtosecond laser pulses and coherent two-phonon Raman scattering were used to excite KTaO$_3$ into a squeezed state, nearly periodic in time, in which the variance of the atomic displacements dips below the standard quantum limit for half of a cycle. This nonclassical state involves a continuum of transverse acoustic modes that leads to oscillations in the refractive index associated with the frequency of a van Hove singularity in the phonon density of states.

Squeezing refers to a class of quantum mechanical states of the electromagnetic field and, more generally, of harmonic oscillators for which the fluctuations in two conjugate variables oscillate out of phase and become alternatively squeezed below the values for the vacuum state for some fraction of a cycle (*1*). Thus, a squeezed electromagnetic field provides a way for experimental measurements to overcome the standard quantum limit for noise imposed by vacuum fluctuations. As such, the generation of squeezed light with various nonlinear processes has attracted much attention as a means of reducing noise in optical interferometry and light-communication networks (*1*).

Following the work on photons (*1*), a variety of intriguing proposals were put forward dealing with squeezed states of other bosons—particularly those associated with atomic vibrations in molecular (*2*) and condensed-matter systems (phonons) (*3*)—as well as polaritons (*4*). In addition, squeezed phonons were considered in variational approaches to the ground state of strongly correlated electron-phonon problems (*5*). Here, we report an experimental demonstration of phonon squeezing in a macroscopic system (*6*). We have generated a squeezed mechanical state by exciting a crystal, KTaO$_3$, with an ultrafast pulse of light. The measurements were performed with the standard pump-probe setup (Fig. 1). Second-order coupling of the photons with the lattice vibrations [specifically, transverse acoustic (TA) modes] amounts to an impulsive change in the phonon frequency that gives rise to squeezing; this mechanism is closely related to that used to generate two-photon coherent states in quantum optics (*7*). We monitored the squeezed state by measuring the transmission of a second (probe) pulse that is sensitive to changes in the refractive index arising from the modulations in the mean square displacement of the atomic positions. Our state comprises a continuum of modes, but the probe transmission is dominated by a single frequency associated with a van Hove singularity in the phonon density of states.

The Hamiltonian relevant to our problem is $H = \Sigma_q(H_q + U_q)$, where $H_q = (P_q^2 + \Omega_q^2\, Q_q^2\,)/2$ is the harmonic contribution to the lattice energy and (*8, 9*)

$$U_q = -\frac{1}{4}\mathcal{P}\,(\mathbf{q})F^2Q_q^2 \qquad (1)$$

Here, Q_q is the amplitude of the phonon of frequency Ω_q and wave vector $\mathbf{q}$, P_q is the associated canonical momentum, F is the magnitude of the electric field, $\mathcal{P} = \Sigma_{ij}\mathcal{P}_{ij}e_ie_j$, $\mathcal{P}_{ij}(\mathbf{q})$ is the second-order polarizability tensor associated with Raman scattering (RS), and $\mathbf{e} = \mathbf{F}/F$ is a unit vector (for clarity, we omit the phonon branch index). Equation 1 describes an effective interaction between two phonons of opposite momenta and two photons and reflects the quadratic term in an expansion of the electronic susceptibility in powers of atomic displacements (*10*).

The generation of the squeezed state is best understood at temperature $T = 0$. Let E denote the pump field, and consider the assumption, valid in our experiments, that the period of the relevant phonons is large compared with both the time it takes for the pulse to cross the sample and the optical pulse width τ_0, that is, we ignore the dependence of the field on position and approximate $F^2 = E^2(t) = (4\pi I_0/n_Rc)\delta(t)$ in Eq. 1 (I_0 is the integrated intensity of the pulse, n_R is the refractive index, c is the speed of the light, and δ is the Dirac delta function). Then, if ψ_q^- is the wave function (the ground state) of a given mode at $t = 0^-$ immediately before the pulse strikes, integration of the Schrödinger equation gives the wave function at $t = 0^+$

$$\psi_q^+ = \exp\left(\frac{i\xi_q\Omega_qQ_q^2}{\hbar}\right)\psi_q^- \qquad (2)$$

where $\xi_q = (\pi I_0\mathcal{P}/2cn_R\Omega_q)$ and $\hbar$ is Planck's constant divided by 2π. It follows that $\langle Q_q(t)\rangle = 0$ (the brackets denote expectation value). We use the equation of motion for Q_q^2 and the initial conditions from Eq. 2 to obtain the variance

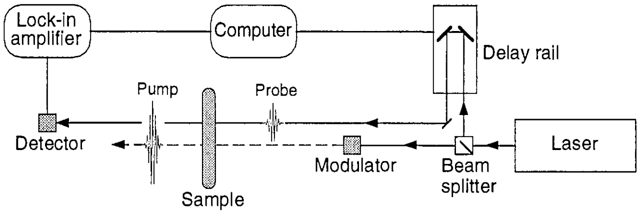

Fig. 1. Schematic snapshot diagram of the experiment (not to scale). The stronger pump pulse drives the sample into an excited time-varying state, which perturbs the weaker probe pulse that follows behind. Here, the signal of interest is the transmitted intensity of the probe beam as a function of the time delay τ, as measured by the relative distance between the two pulses.

G. A. Garrett, A. K. Sood, R. Merlin, Center for Ultrafast Optical Science, University of Michigan, Ann Arbor, MI 48109-2099, and Department of Physics, University of Michigan, Ann Arbor, MI 48109-1120, USA.
A. G. Rojo, Department of Physics, University of Michigan, Ann Arbor, MI 48109-1120, USA.
J. F. Whitaker, Center for Ultrafast Optical Science, University of Michigan, Ann Arbor, MI 48109-2099, USA.

*On leave from Department of Physics, Indian Institute of Science, Bangalore 560 012, India.

†To whom correspondence should be addressed.